J|A|C|S
ARTICLES
Published on Web 05/03/2002

Nature of the Intermediate Formed in the Reduction of O_2 to H_2O at the Trinuclear Copper Cluster Active Site in Native Laccase

Sang-Kyu Lee,[†] Serena DeBeer George,[†] William E. Antholine,[‡] Britt Hedman,[†,§] Keith O. Hodgson,[†,§] and Edward I. Solomon*[,†]

Contribution from the Department of Chemistry, Stanford University, Stanford, California 94305, Medical College of Wisconsin, the Biophysics Research Institute, National Biomedical ESR Center, Milwaukee, Wisconsin 53226, and Stanford Synchrotron Radiation Laboratory, SLAC, Stanford University, Stanford, California 94309

Received June 7, 2001. Revised Manuscript Received January 3, 2002

Abstract: The multicopper oxidases contain at least four copper atoms and catalyze the four-electron reduction of O_2 to H_2O at a trinuclear copper cluster. An intermediate, termed native intermediate, has been trapped by a rapid freeze-quench technique from *Rhus vernicifera* laccase when the fully reduced form reacts with dioxygen. This intermediate had been described as an oxygen-radical bound to the trinuclear copper cluster with one Cu site reduced. XAS, however, shows that all copper atoms are oxidized in this intermediate. A combination of EXAFS, multifrequency EPR, and VTVH MCD has been used to understand how this fully oxidized trinuclear Cu cluster relates to the fully oxidized resting form of the enzyme. It is determined that in the native intermediate all copper atoms of the cluster are bridged by the product of full O_2 reduction. In contrast, the resting form has one copper atom of the cluster (the T2 Cu) magnetically isolated from the others. The native intermediate decays to the resting oxidized form with a rate that is too slow to be in the catalytic cycle. Thus, the native intermediate appears to be the catalytically relevant fully oxidized form of the enzyme, and its role in catalysis is considered.

I. Introduction

The multicopper oxidases,[1−5] which include laccase (Lc), ascorbate oxidase (AO), ceruloplasmin (Cp), and Fet3, catalyze the four-electron reduction of O_2 to H_2O according to eq 1.

$$O_2 + 4e^- + 4H^+ \xrightarrow[4Cu^{2+}]{} 2H_2O \qquad (1)$$

Lc is the simplest of these multicopper oxidases having only four copper atoms in its active site.

The metal centers in the multicopper oxidases are classified into three types according to their spectroscopic characteristics. The type 1 (T1) center, which is the substrate reaction site, is characterized by an intense blue absorption feature at 614 nm ($\epsilon = 5300\ M^{-1}\ cm^{-1}$) arising from Cys S → Cu charge-transfer (CT) transitions as well as an EPR signal with a small hyperfine coupling ($g_{||} = 2.30$, $A_{||} = 39 \times 10^{-4}\ cm^{-1}$). The Cys ligand at the T1 Cu is flanked on either side in the sequence by histidines, which are ligands to the Cu atoms at the binuclear type 3 (T3) center. The T3 center contains two antiferromagnetically coupled copper atoms and exhibits a characteristic 330 nm absorption band arising from CT transitions of a bridging OH to the Cu(II)s. The oxidized type 2 (T2) center is three coordinate and exhibits a normal Cu(II) EPR signal ($g_{||} = 2.24$, $A_{||} = 182 \times 10^{-4}\ cm^{-1}$). The T2 center is labile, and reduction in the presence of a chelator can selectively remove this copper ion generating the T2 depleted (T2D) derivative.[6−9] The T2 and T3 centers are close together and form a trinuclear cluster, which is the site of dioxygen reduction. Crystal structures of AO[10−12] and Cp[13−15] revealed that this center is separated from the T1 center by about 13 Å.

* To whom correspondence should be addressed. E-mail: Edward.Solomon@stanford.edu.
[†] Department of Chemistry, Stanford University.
[§] Stanford Synchrotron Radiation Laboratory, Stanford University.
[‡] Medical College of Wisconsin, The National Biomedical EPR Center.

(1) Reinhammar, B. In *Copper Proteins and Copper Enzymes*; Lontie, R., Ed.; CRC Press: Boca Raton, FL, 1984; Vol. 3, pp 1−35.
(2) Messerschmidt, A. In *Multi-copper Oxidases*; Messerschmidt, A., Ed.; World Scientific: Singapore; River Edge, NJ, 1997; pp 23−80.
(3) Malmström, B. G.; Reinhammar, B.; Vänngård, T. *Biochim. Biophys. Acta* **1968**, *156*, 67−76.
(4) Solomon, E. I.; Baldwin, M. J.; Lowery, M. D. *Chem. Rev.* **1992**, *92*, 521−542.
(5) Solomon, E. I.; Sundaram, U. M.; Machonkin, T. E. *Chem. Rev.* **1996**, *96*, 2563−2605.
(6) Li, J. B.; McMillin, D. R. *Biochim. Biophys. Acta* **1992**, *1160*, 239−245.
(7) Hanna, P. M.; McMillin, D. R.; Pasenkiewicz-Gierula, M.; Antholine, W. E.; Reinhammar, B. *Biochem. J.* **1988**, *253*, 561−568.
(8) Graziani, M. T.; Morpurgo, L.; Rotilio, G.; Mondovi, B. *FEBS Lett.* **1976**, *70*, 87−90.
(9) Malkin, R.; Malmström, B. G.; Vänngård, T. *Eur. J. Biochem.* **1969**, *7*, 253−259.
(10) Messerschmidt, A.; Rossi, A.; Ladenstein, R.; Huber, R.; Bolognesi, M.; Gatti, G.; Marchesini, A.; Petruzzelli, R.; Finazzi-Agro, A. *J. Mol. Biol.* **1989**, *206*, 513−529.
(11) Messerschmidt, A.; Ladenstein, R.; Huber, R.; Bolognesi, M.; Avigliano, L.; Petruzzelli, R.; Rossi, A.; Finazzi-Agro, A. *J. Mol. Biol.* **1992**, *224*, 179−205.
(12) Messerschmidt, A.; Luecke, H.; Huber, R. *J. Mol. Biol.* **1993**, *230*, 997−1014.

10.1021/ja0114052 CCC: $22.00

Scheme 1

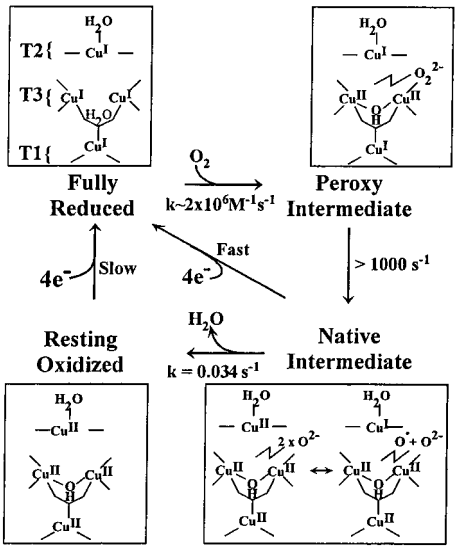

Spectroscopic and kinetic properties of *Rhus vernicifera* Lc isolated from the Japanese lacquer tree make this enzyme ideal for a detailed study of the dioxygen reduction mechanism. Past studies of this reaction in different forms of Lc have demonstrated the presence of two intermediate species termed the peroxy intermediate[16−18] and the native intermediate.[19−22] Scheme 1 summarizes our current working model of the reaction mechanism. The fully reduced trinuclear copper cluster site reacts with dioxygen to generate the peroxy intermediate. This intermediate has been trapped and extensively studied[18] using the T1 Hg derivative of Lc in which the T1 copper has been replaced with a redox inactive mercuric ion.[23,24] The peroxy intermediate decays to the resting oxidized T1Hg Lc via a species similar to the native intermediate.[18] In the native enzyme, the peroxy intermediate would be produced transiently in the formation of the native intermediate. The oxygen species in the native intermediate is at least $1e^-$ further reduced than that in the peroxy intermediate, as the T1 Cu is now present and oxidized in its formation.

It had been proposed that in the native intermediate, the T2 copper is reduced, and an oxyl or hydroxyl radical is bound to an oxidized T3 center.[19,21,25,26] The proposal was based on the fact that the EPR signal associated with the oxidized T2 center is not present in the native intermediate. Further, a broad EPR signal with a g value below 2.00 is observed (at <20 K), and this shows additional broadening with $^{17}O_2$.[27] Our preliminary spectroscopic results on the native intermediate suggested that all of the copper ions were in fact oxidized.[22] This study examines the electronic and magnetic properties of the native intermediate in detail by a combination of stopped-flow absorption and rapid-freeze-quench (RFQ) X-ray absorption spectroscopy (XAS), multifrequency electron paramagnetic resonance (EPR), and variable-temperature variable-field magnetic circular dichroism (VTVH MCD). The structure and origin of the unusual spectroscopic properties of this intermediate are defined in terms of an all-bridged trinuclear Cu(II) cluster. The relation of this fully oxidized intermediate structure to the resting oxidized site is determined and extended to the catalytic mechanism.

II. Experimental Methods

Chemicals and Protein Preparation. All chemicals were reagent grade and used without further purification. Water was purified using a Barnstead Nanopure deionizing system. *Rhus vernicifera* laccase (*p*-diphenol:dioxygen oxidoreductase, EC 1.10.3.2) was isolated from acetone powder (Saito and Co., Osaka, Japan) and assayed according to published procedures.[28,29] T2D was prepared as described previously.[8,9,30] The protein concentration was determined using the extinction coefficient ($\epsilon_{280} = 90\,000\ M^{-1}\ cm^{-1}$) of the absorption band at 280 nm.[28,29,31] Copper concentration was determined spectrophotometrically using 2,2′-biquinoline.[32,33]

UV/Vis Absorption and MCD Spectroscopy. UV/visible absorption spectra were recorded on a Hewlett-Packard HP8452A diode array spectrophotometer. Rapid scan stopped-flow experiments were performed on an Applied Photophysics SX.18MV, stopped-flow absorption spectrophotometer equipped with a PDA.1 Photodiode Array accessory. MCD spectra were recorded in the UV/visible region using Jasco J500 or J810 spectropolarimeters equipped with S-1 and S-20 photomultiplier tubes for the 1050−800 and 800−300 nm regions, respectively. In the near-IR region, MCD spectra were recorded using a Jasco J200 spectropolarimeter equipped with a liquid-nitrogen cooled InSb solid-state detector. Each instrument was modified to accommodate magnetocryostats, Oxford SM-4 (7 T, UV/Vis) or SM-4000 (7 T, near-IR), superconducting magnets with optical access within their sample compartments. MCD data were obtained using a sample cell consisting of two infrasil quartz disks with a 3 mm neoprene spacer.

Iterative, simultaneous Gaussian fits to the room-temperature absorption and LT MCD spectra were carried out using the program PeakFit version 4 (AISN Software Inc.). The MCD temperature dependence was fit and the energy matrix calculated by macro scripts written for Excel 97 (Microsoft Corp.) or Mathcad 7.0 (MathSoft Inc.).

Multifrequency EPR Spectroscopy. All X-band (9.2 GHz) spectra were obtained with a Bruker ER 220-D-SRC spectrometer. Sample temperatures of 77 K were maintained using a liquid N_2 coldfinger dewar, and temperatures from 70 to 4 K were obtained using an Air Products Model LTR Helitran liquid helium transfer refrigerator and a Lake Shore Cryotronics temperature controller Model DTC-500. S-band (3.4 GHz) spectra were obtained from a spectrometer with a loop-gap

(13) Zaitsev, V.; Zaitseva, I.; Papiz, M.; Lindley, P. F. *J. Biol. Inorg. Chem.* **1999**, *4*, 579−587.
(14) Zaitseva, I.; Zaitsev, V.; Card, G.; Moshkov, K.; Bax, B.; Ralph, A.; Lindley, P. *J. Biol. Inorg. Chem.* **1996**, *1*, 15−23.
(15) Lindley, P. F.; Card, G.; Zaitseva, I.; Zaitsev, V.; Reinhammar, B.; Selin-Lindgren, E.; Yoshida, K. *J. Biol. Inorg. Chem.* **1997**, *2*, 454−463.
(16) Cole, J. L.; Ballou, D. P.; Solomon, E. I. *J. Am. Chem. Soc.* **1991**, *113*, 8544−8546.
(17) Cole, J. L.; Tan, G. O.; Yang, E. K.; Hodgson, K. O.; Solomon, E. I. *J. Am. Chem. Soc.* **1990**, *112*, 2243−2249.
(18) Shin, W.; Sundaram, U. M.; Cole, J. L.; Zhang, H. H.; Hedman, B.; Hodgson, K. O.; Solomon, E. I. *J. Am. Chem. Soc.* **1996**, *118*, 3202−3215.
(19) Aasa, R.; Brändén, R.; Deinum, J.; Malmström, B. G.; Reinhammar, B.; Vänngård, T. *FEBS Lett.* **1976**, *61*, 115−119.
(20) Andréasson, L.-E.; Brändén, R.; Malmström, B. G.; Vänngård, T. *FEBS Lett.* **1973**, *32*, 187−189.
(21) Andréasson, L.-E.; Brändén, R.; Reinhammar, B. *Biochim. Biophys. Acta* **1976**, *438*, 370−379.
(22) Clark, P. A.; Solomon, E. I. *J. Am. Chem. Soc.* **1992**, *114*, 1108−1110.
(23) Moriebebel, M. M.; McMillin, D. R.; Antholine, W. E. *Biochem. J.* **1986**, *235*, 415−420.
(24) Moriebebel, M. M.; Morris, M. C.; Menzie, J. L.; McMillin, D. R. *J. Am. Chem. Soc.* **1984**, *106*, 3677−3678.
(25) Huang, H. W.; Zoppellaro, G.; Sakurai, T. *J. Biol. Chem.* **1999**, *274*, 32718−32724.
(26) Brändén, R.; Deinum, J. *Biochim. Biophys. Acta* **1978**, *524*, 297−304.
(27) Aasa, R.; Brändén, R.; Deinum, J.; Malmström, B. G.; Reinhammar, B.; Vänngård, T. *Biochem. Biophys. Res. Commun.* **1976**, *70*, 1204−1209.
(28) Reinhammar, B. *Biochim. Biophys. Acta* **1970**, *205*, 35−47.
(29) Reinhammar, B. *Biochim. Biophys. Acta* **1972**, *275*, 245−259.
(30) Reinhammar, B.; Oda, Y. *J. Inorg. Biochem.* **1979**, *11*, 115−127.
(31) Meadows, K. A.; Moriebebel, M. M.; McMillin, D. R. *J. Inorg. Biochem.* **1991**, *41*, 253−260.
(32) Hanna, P. M.; Tamilarasan, R.; McMillin, D. R. *Biochem. J.* **1988**, *256*, 1001−1004.
(33) Felsenfeld, G. *Arch. Biochem. Biophys.* **1960**, *87*, 247−251.

resonator cavity and a low-frequency microwave bridge built at the National Biomedical ESR Center, Medical College of Wisconsin. Spin quantification of protein samples was determined using a Cu standard (1.0 mM $CuSO_4 \cdot 5H_2O$ with 2 mM HCl and 2 M $NaClO_4$).

Intermediate Sample Preparation. All intermediate sample concentrations were 0.4 mM protein in either 100 mM phosphate or 100 mM MOPS buffer at pH 7.5, 4 °C unless otherwise noted. Typically, laccase samples were made anaerobic in a conically bottomed reaction vial by gently flushing with O_2-scrubbed Ar gas on Schlenk lines for 30 min at 4 °C. Degassed four-electron equivalents of ascorbate were then added to the reaction mixture and allowed to equilibrate for an additional 30 min. Reductants (ascorbate or dithionite) in slight excess were added to maintain strict anaerobic conditions. The reaction mixture was then loaded into a 1.0 mL stopped-flow syringe. O_2-saturated buffer solution (1.4 mM at 4 °C) was also loaded into a second 1.0 mL stopped-flow syringe. The two syringes were then assembled for rapid mixing with an Update Instruments System 1000 equipped with a Wiskind Grid Mixer. RFQ EPR and XAS samples were frozen by spraying directly into liquid N_2 or into liquid N_2 chilled isopentane at −140 °C. The frozen samples were then packed into either 4 mm quartz EPR tubes or XAS sample holders. RFQ MCD samples were made by transferring the frozen samples into chilled glycerol in a reaction vial submersed in an ethanol/dry ice bath at −30 °C. The frozen samples were then dissolved by thoroughly mixing into glycerol at −30 °C and transferred quickly using a chilled Hamiltion syringe to a MCD cell kept at −30 °C. The transferring process was completed within 2 min. The extent of the intermediate decay was determined by measuring the EPR signal before and after dissolving in glycerol and was found to be negligible.

XAS Sample Preparation. The Cu concentrations for the reduced, fully oxidized, and native intermediate samples were 6.0, 4.0, and 1.6−2.4 mM, respectively, all in phosphate and/or MOPS buffer at pH 7.5. Seven separate preparations of the native intermediate were run. The data presented represent both the highest concentration and the highest percentage yield of native intermediate based on EPR quantitation. All native intermediate samples were prepared by freeze-quench techniques. As a control, fully oxidized samples were prepared both by freeze-quench and as solutions with ∼20% glycerol. The fully reduced sample was prepared as a solution with ∼20% glycerol. Freeze-quenched samples were packed into windowless Lucite XAS cells holders and inserted into 2- mm Lucite XAS cells with 63.5 μm Mylar windows. Solution samples were loaded into 1 mm Lucite XAS cells with 63.5 μm Mylar windows. All samples were frozen immediately by immersion in liquid nitrogen and kept at this temperature or lower throughout.

XAS Data Acquisition. All data were collected at the Stanford Synchrotron Radiation Laboratory (SSRL) on unfocused 8-pole wiggler beam line 7-3 under ring conditions 3.0 GeV and 60−100 mA. A Si(220) monochromator was utilized for energy selection with the monochromator detuned 50% to minimize higher harmonic components in the X-ray beam. The samples were maintained at 10 K during the data collection using an Oxford Instruments CF1208 continuous-flow liquid helium cryostat. Data were measured in fluorescence mode using a Canberra Ge 13-element array detector. Internal energy calibration was performed by simultaneous measurement of the absorption of a Cu foil placed between a second and third ionization chamber. The first inflection point of the Cu foil was assigned to 8980.3 eV.

XAS Data Reduction. All samples were monitored for photoreduction throughout the course of data collection. Only those scans which showed no evidence of photoreduction were used for edge comparisons. For the EXAFS analysis, only scans which showed less than 5% photoreduction were averaged. All freeze-quenched samples were found to contain some ice, and a small amount was also present in the ∼20% glycerol solution samples. For this reason, single channel averages were examined for ice diffraction. It was found that in most of the channels there was some interference from ice at high k; hence the data have been truncated beyond $k = 11$ Å^{-1}. Those channels which showed contributions from ice diffraction below $k = 11$ Å^{-1} were not included in the average. The data represent 16-scan averages for both the reduced and the fully oxidized, and a 20-scan average for the native intermediate.

The averaged data were processed as described previously[34] by fitting a second-order polynomial to the post-edge region and subtracting this background from the entire spectrum. A three-region cubic spline was used to model the smooth background above the edge. Normalization of the data was achieved by subtracting the spline and normalizing the edge jump to 1.0 at 9000 eV. The resultant EXAFS was k^3-weighted to enhance the impact of high-k data.

XAS Data Analysis. The Cu K-edge of the native intermediate was analyzed through comparisons with the reduced and fully oxidized laccase edges. By subtracting the normalized edge of fully oxidized laccase from that of reduced laccase, a characteristic derivative shape signal is produced, the amplitude of which corresponds to 100% reduced laccase. Performing a similar subtraction of the fully oxidized data from the native intermediate data allows quantitation of the percent of reduced copper present in the native intermediate.

Theoretical EXAFS signals $\chi(k)$ were calculated using FEFF (version 6.0)[35,36] and fit to the data using EXAFSPAK.[37] The experimental energy threshold, E_0 (the point at which $k = 0$), was chosen as 9000 eV. The ΔE_0 represents the deviation from this value. The structural parameters varied during the refinements were the bond distance (R) and the bond variance (σ^2). The σ^2 is related to the Debye−Waller factor, which is a measure of thermal vibration and static disorder of the absorbers/scatterers. Coordination numbers were systematically varied in the course of the analysis, but they were not allowed to vary within a given fit. Single scattering paths and the corresponding multiple scattering paths were linked during the course of refinements.

III. Results and Analysis

1. Formation and Decay of the Native Intermediate. The rapid scan stopped-flow absorption spectrum of the native intermediate of tree laccase (Figure 1) exhibits features with apparent maxima at 315, 365, and 614 nm. This intermediate species is observed when four-electron reduced laccase is rapidly mixed with O_2-saturated buffer. The fully reduced laccase spectrum is digitally subtracted from the experimental data to eliminate scattering and the contribution from the protein. Figure 1A and C shows the apparent pseudo-first-order formation of the native intermediate with a rate constant of ∼700 s^{-1} ([O_2] = 0.7 mM, pH 7.5 and 4 °C). This formation step was previously shown to be an O_2-dependent second-order process (1.6×10^6 s^{-1} M^{-1}).[16,21] Figure 1B and C shows the apparent first-order decay of the native intermediate at 6.6×10^{-3} s^{-1} ($t_{1/2} = 104$ s) at 4 °C. In earlier studies, the reported decay rate is $\sim 5 \times 10^{-2}$ s^{-1} ($t_{1/2} \approx 13$ s) at 25 °C.[21]

The appearance of the blue band at 614 nm in the native intermediate, identical to that in the resting oxidized state, indicates the T1 center is oxidized in the native intermediate.[19,21] Figure 2A shows the 77 K X-band EPR spectrum of the native intermediate prepared by RFQ (aged for 25 ms at 4 °C). The spectrum exhibits a typical oxidized T1 copper signal with $g_{||} = 2.30$ and $A_{||} = 39 \times 10^{-4}$ cm^{-1}, similar to that of the resting oxidized laccase shown in Figure 2B. Unlike the resting oxidized laccase, however, the native intermediate lacks the T2 Cu EPR

(34) DeWitt, J. G.; Bentsen, J. G.; Rosenzweig, A. C.; Hedman, B.; Green, J.; Pilkington, S.; Papaefthymiou, G. C.; Dalton, H.; Hodgson, K. O.; Lippard, S. J. *J. Am. Chem. Soc.* **1991**, *113*, 9219−9235.
(35) Rehr, J. J.; Mustre de Leon, J.; Zabinsky, S. I.; Albers, R. C. *J. Am. Chem. Soc.* **1991**, *113*, 5135−5140.
(36) Mustre de Leon, J.; Rehr, J. J.; Zabinsky, S. I.; Albers, R. C. *Phys. Rev. B* **1991**, *44*, 4146−4156.
(37) George, G. N. Stanford Synchrotron Radiation Laboratory, SLAC, Stanford University: Stanford, CA 94309.

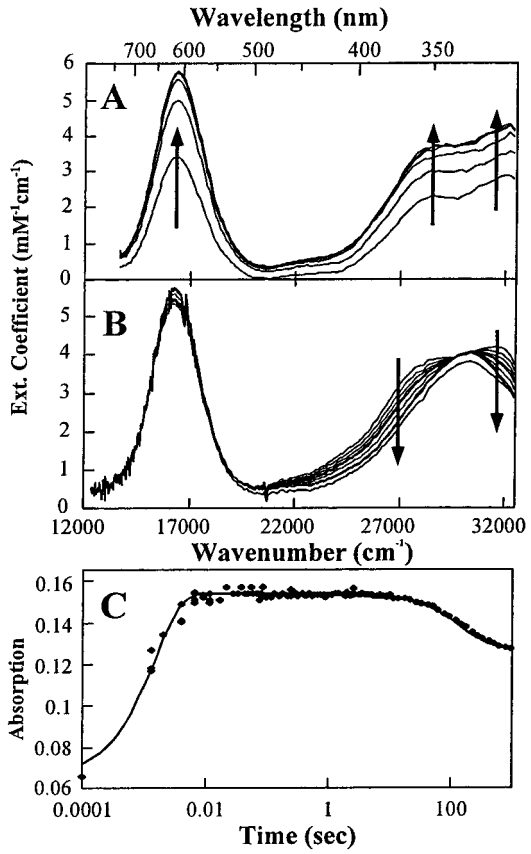

Figure 1. Formation and decay of the native intermediate (monitored using a rapid scan stopped-flow instrument at pH 7.5 and 4 °C). (A) The first scan after mixing is at 1.28 ms, and each successive scan is taken every 2.56 ms up to 11.52 ms. (B) The decay of the native intermediate scans at 0.017, 0.30, 0.57, 0.83, 1.0, 1.5, 5, 13, 20, and 30 min. (C) The time course of the native intermediate formation and decay.

signal (Figure 2A and C). The absence of the T2 EPR signal had been interpreted as indicating that the T2 Cu center is reduced in the native intermediate.

The features at 316 and 364 nm appear concomitant with the blue band as shown in Figure 1A. This suggests that the oxidation of the T1 center and the formation of 316 and 364 nm bands occur in one step or without accumulation of other transient species. These bands at 316 and 364 nm disappear with time, and the resulting absorption spectrum of the decayed product resembles that of oxidized laccase with a broad band at 330 nm as well as the blue band at 614 nm (Figure 1B). The absorption band at 330 nm has been associated with the formation of the oxidized T3 coupled binuclear site. The new absorption features at 316 and 364 nm are intense, indicating that these are ligand to metal charge-transfer (LMCT) transitions. In this energy region (25 000−30 000 cm^{-1}), these should be OH^- (or oxo, vide infra) CT transitions to oxidized Cu ions of the trinuclear cluster.[38]

2. Multifrequency EPR Spectroscopy. Native Intermediate EPR Spectrum. The X-band EPR spectrum of the native intermediate obtained at 10 K and low microwave power is shown in Figure 2C. As expected, the T1 signal saturates as the applied power is progressively increased from 0.5 to 25 μW. However, upon increasing the power to 0.1 mW or higher at

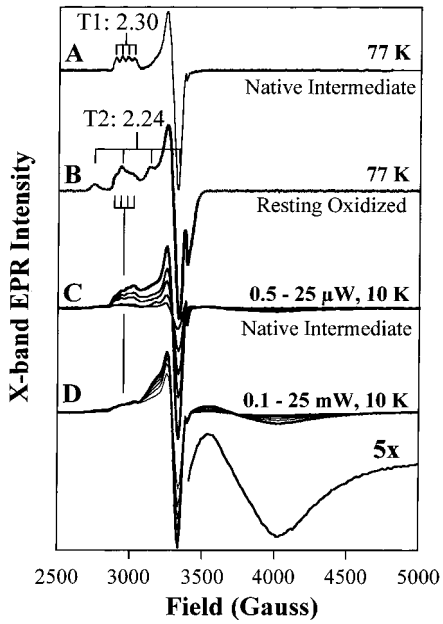

Figure 2. (A) EPR spectrum of the native intermediate at 2.02 mW and 77 K. (B) EPR spectrum of the resting oxidized form at 2.02 mW and 77 K. (C) EPR spectra of the native intermediate taken at 0.5−25 μW at 10 K. (D) EPR spectra of the native intermediate showing a new broad feature around 4000 G taken at 0.1−25 mW at 10 K, 9.5 GHz, 10 G (mod. amp.), and 100 kHz (mod. freq.).

10 K, a new shoulder around 3200 G and a broad feature around 4000 G become visible (Figure 2D). Consistent with previous findings,[19,21] the new signal can be detected only at low temperature (<20 K) and at high power (>0.1 mW). Figure S1A shows the EPR spectrum of the native intermediate measured at 5 K and 200 mW. This spectrum contains contributions from the saturated T1 Cu axial signal and from the new broad feature of the native intermediate. Low temperature and high power were used to maximize the intensity of the broad signal. At this setting, the T1 signal is almost saturated. To remove the spectral contribution from the T1 signal, the EPR spectrum of T2D under the same conditions was obtained (Figure S1B) and subtracted from the native intermediate spectrum. The spectrum of T2D also shows a heavily saturated T1 copper signal as shown in Figure S1B. In addition to spectral contributions from T1 copper, the native intermediate spectrum in Figure S1A exhibits a very small radical signal (<1%). There is no correlation between the amounts of radical species formed among various sample preparations; it appears to be associated with variable amounts of excess substrate in the different preparations. The radical signal was also digitally removed from the native intermediate spectrum. Figure S1C shows the resulting broad spectrum with its simulated spectrum overlaid.[39] Simulations showed that the EPR signal is rhombic and has $g_{(max,\ mid,\ min)}$ of 2.15, 1.86, and 1.65, respectively.

The S-band EPR spectrum with simulation of the native intermediate shown in Figure S1D was obtained by subtracting the T1 Cu signal in a similar manner. Simulation of the S-band EPR spectrum gave the same set of g values, 2.15, 1.86, and 1.65. Only the line widths of the bands were adjusted to account for their known frequency dependence. The simulated EPR

(38) Spira-Solomon, D. J.; Solomon, E. I. *J. Am. Chem. Soc.* **1987**, *109*, 6421−6432.

(39) The residual T1 signal at the low field region is due to the differences in the relaxation behavior of the perpendicular and parallel region in T2D and in the native intermediate. The origin of this behavior is not known.

Table 1. Multifrequency EPR Simulation Parameters

frequency	parameters	g_{max}	g_{mid}	g_{min}
X-band (9.5 GHz)	g_{eff}	2.15	1.86	1.65
	A_{eff},[a] $\times 10^{-4}$ cm^{-1}	30	45	73
	line width,[a] $\times 10^{-4}$ cm^{-1}	17	63	53
S-band (3.5 GHz)	g_{eff}	2.15	1.86	1.65
	A_{eff},[a] $\times 10^{-4}$ cm^{-1}	30	45	73
	line width,[a] 10^{-4} cm^{-1}	8	32	27

[a] A_{eff} and line widths shown indicate minimum values required to simulate the broad unresolved hyperfines.

parameters are summarized in Table 1. Because of the lack of resolvable hyperfine structure in the EPR signal, the simulated hyperfine parameters only reflect effective values, accounting for contributions from all $I > 0$ nuclei.

Previously, it had been reported that the broad EPR feature of the native intermediate changed with pH, which was proposed to be a protonation event.[26,40] However, we have found that this reported "pH effect" is in fact due to the change in buffer.[41] In the previous studies, the EPR spectrum of the native intermediate showed significant differences when samples made in Na-acetate (pH 5.5, Figure S2A) were compared to those made in Na-phosphate (pH 7.5, Figure S2B). Particularly, the broad feature around 4000 G shifts to lower field and sharpens with low pH in acetate buffer. However, when the native intermediate sample is made in Na-MES (pH 5.5, Figure S2C) or in Na-MOPS (pH 7.5, Figure S2D), the resulting EPR spectra show no differences relative to that prepared in Na-phosphate buffer at pH 7.5 (Figure S2B).

Power Saturation and Orbach Analysis. An important characteristic of the native intermediate EPR spectrum is that this broad signal is very difficult to saturate, which suggests the presence of a novel relaxation pathway. Figure S3A shows progressive microwave power saturation data for the native intermediate between 9 and 17 K. The signal intensities are measured at 4000 G, and the saturation behavior of the native intermediate is analyzed according to the following equation.[42]

$$\frac{I}{\sqrt{P}} = \frac{1}{[1 + (P/P_{1/2})]^{b/2}} \tag{2}$$

where I is the intensity of the signal at 4000 G, P is the microwave power, $P_{1/2}$ is the microwave power at half-saturation, and b is the inhomogeneity parameter. For the first derivative EPR spectrum, b is 1 in the inhomogeneous limit and 3 in the homogeneous limit. Most EPR signals in proteins are inhomogeneously broadened such that b should be near 1. From Table S1, the power saturation studies show that the broad EPR signal associated with the native intermediate is much more difficult to saturate than is the T1 EPR signal. The $P_{1/2}$ of the native intermediate EPR signal at 8.8 K is >25 mW, although the half-saturation point of the T1 EPR signal is approximately 0.45 mW and that of the T2 EPR signal is approximately 0.05 mW.

Equation 3 relates the half-power saturation process to the relaxation rates of energy redistribution following the microwave absorption.

$$P_{1/2} \propto \frac{1}{T_1 \cdot T_2} \tag{3}$$

where T_1^{-1} is the spin−lattice relaxation rate, and T_2^{-1} is the spin−spin relaxation rate. The spin−lattice relaxation process involves energy redistribution from a paramagnetic center to its surrounding, whereas the spin−spin relaxation process involves redistribution within the spin system. The T_2 process does not significantly influence the temperature dependence of the $P_{1/2}$ value, and the T_1 process becomes the dominant factor in the temperature range studied here. In a magnetically insulated protein active site, an additional efficient relaxation pathway is via a low-lying excited state. This Orbach process is described by eq 4.

$$1/T_1 \propto e^{-\Delta/k_B \cdot T} \tag{4}$$

where k_B is the Boltzmann constant ($k_B = 0.695$ cm^{-1} K^{-1}), and Δ is the energy gap between the ground and the excited state in cm^{-1}. Thus, $P_{1/2}$ is related to the Δ value by eq 5.

$$\ln P_{1/2} \propto -\Delta/k_B \cdot T \tag{5}$$

The saturation data and simulations at 4000 G and various temperature settings between 9 and 17 K are shown in Figure S3A. The Orbach analysis shown in Figure S3B reveals a linear relationship, and the slope of the line directly relates to the energy separation of the low-lying excited state. The slope gives $\Delta = 140 \pm 30$ cm^{-1}. Thus, the saturation behavior of the native intermediate EPR signal is due to the presence of a low-lying excited state[43] at ~140 cm^{-1}.

The presence of a low-lying excited state is very unusual. For Cu(II) monomers, the lowest excited states are in the 5000 cm^{-1} (T1) or 10 000 cm^{-1} (T2) energy region, consistent with the relatively slow relaxation. In addition, large g and A values are generally observed for Cu(II) monomers. These unique EPR features associated with the native intermediate require that the signal be of a novel species. Initially, it had been thought to be associated with an OH$^{\bullet}$ radical, which would require the T2 copper atom to be reduced.

3. Cu K-Edge XAS and EPR Quantitation of Cu(I) and Cu(II). A comparison of the normalized Cu K-edge spectra of the reduced, fully oxidized, and native intermediate forms of laccase is shown in Figure 3A. Fully reduced laccase exhibits an intense 1s → 4p transition at ~8984 eV, which is characteristic of Cu(I) in a three-coordinate environment.[44] In contrast, fully oxidized laccase exhibits no peak maximum below 8985.0 eV, except a very weak 1s → 3d pre-edge transition at ~8979 eV. Using the Cu K-edge of reduced laccase minus that of fully oxidized laccase as reference for 100% reduced copper (Figure 3B), the amount of Cu(I) in a given native intermediate sample can be quantified through an edge difference comparison assuming all Cu(I) sites have a similar contribution, that is, three coordinate as in the X-ray structure of the reduced trinuclear site.[12] In the seven separate preparations of the native intermediate, it was found that ~8−28% of all copper was reduced (Table 2, data/Cu(I)$_{tot}$). Much of the variation was due to the presence

(40) Huang, H. W.; Sakurai, T.; Monjushiro, H.; Takeda, S. *Biochim. Biophys. Acta* **1998**, *1384*, 160−170.
(41) Sundarm, U. W. Thesis work, Stanford University, 1997.
(42) Poole, J. C. P. *Electron Spin Resonance: A Comprehensive Treatise on Experimental Techniques*; Wiley: New York, 1983.
(43) A temperature sweep between 10 and 200 K (data not shown) failed to reveal any new EPR features that might be associated with the excited state.
(44) Kau, L. S.; Spira-Solomon, D. J.; Penner-Hahn, J. E.; Hodgson, K. O.; Solomon, E. I. *J. Am. Chem. Soc.* **1987**, *109*, 6433−6442.

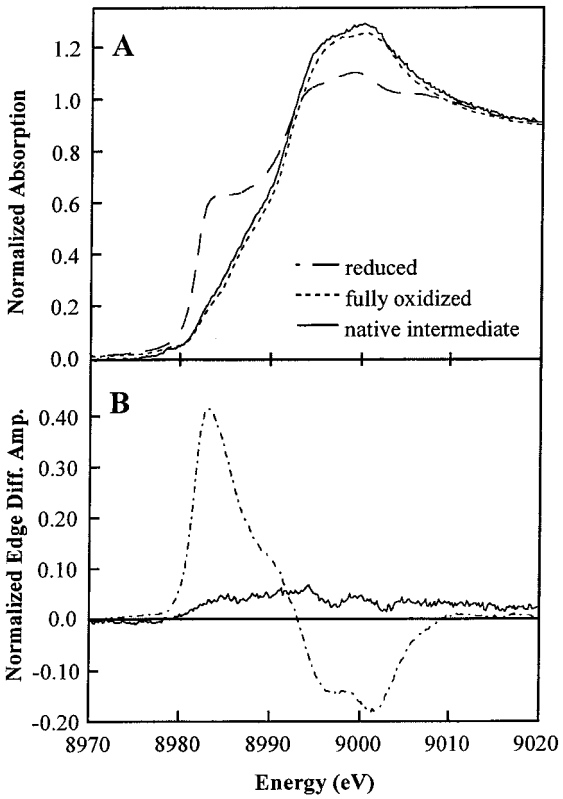

Figure 3. (A) Cu K-edge data for reduced, fully oxidized, and the native intermediate of laccase. (B) The normalized edge difference spectra for fully reduced and the native intermediate of laccase.

of the slight excess of reductant (dithionite or ascorbate), which was added to ensure the anaerobicity of the freeze-quench instrument. This addition caused some re-reduction of the native intermediate and resulted in samples that contain different distributions of the intermediate, re-reduced intermediate (vide infra), unreacted, and decayed product. A combination of XAS and EPR spin quantitation can be used to determine the distribution of these species, where XAS quantitates the total Cu(I), and EPR quantitates the amounts of T1 and T2 Cu(II) present (Table 2, data/$T1_{ox}$ and $T2_{ox}$).

To determine the composition of the intermediate samples, a number of different models were considered (Scheme 2). The first two models (1A, 1B) assume the minimal case in which the sample is comprised of fully reduced, native intermediate, and resting oxidized laccase. The lack of a T2 Cu EPR signal in all cases indicates that no resting oxidized enzyme is present. In this case, the oxidized T1 Cu EPR signal quantitates the amount of native intermediate present, and the remainder corresponds to fully reduced enzyme. Using the T1 spin quantitation value from EPR, an expected value for total Cu(I) can be calculated and compared to the experimentally measured value from XAS. Model 1A assumes T2 is reduced in the native intermediate; thus the total Cu(I) will reflect the fully reduced and the T2 site of the native intermediate. The total reduced copper in model 1A is then a sum of the fully reduced form and $^1/_4$ equivalent of the native intermediate. Comparison of the calculated amount of Cu(I) (Table 2, model 1A/$Cu(I)_{cal}$) with the experimentally measured Cu(I) (Table 2, data/$Cu(I)_{tot}$) indicates that this model overestimates the amount of Cu(I) present. Model 1B assumes the native intermediate is fully oxidized, and thus the only Cu(I) present will be in the fully reduced unreacted enzyme. This requires the reduced T1 Cu deduced from EPR spin quantitation (Table 2, model 1B/fRed) to be equal to the total Cu(I) measured from XAS (Table 2, data/$Cu(I)_{tot}$). This model also overestimates the amount of Cu(I) present, and thus the data require inclusion of an additional partially reduced species.

Two additional models (2A, 2B) were considered in which partial re-reduction of the T1 site in the native intermediate was included (Scheme 2). Experimentally measured T1 Cu(II) from EPR spin quantitation and total Cu(I) from XAS are used together to calculate the distribution of the possible species. In model 2A, the T2 Cu site of the native intermediate is assumed to be reduced. Re-reduction of this intermediate leads to a species with both T1 and T2 sites reduced. According to this model, Cu(I) is distributed over the fully reduced, native intermediate, and re-reduced native intermediate species. This model predicts unrealistic percentages, significantly below zero, for the unreacted fully reduced species (Table 2, model 2A/$fRed_{cal}$). Finally, model 2B was considered, in which the native intermediate is assumed to be fully oxidized. Re-reduction of this intermediate leads to a species with only the T1 site reduced. This model with all the copper atoms of the native intermediate oxidized produces a reasonable distribution of species (Table 2, model 2B) and is the only model that is consistent with experimental results.[45] Thus, the native intermediate is best described as a fully oxidized form of the enzyme, and O_2 has been reduced by $4e^-$ to the water level.

4. EXAFS. The k^3-weighted EXAFS data and fits for the reduced, fully oxidized, and native intermediate forms of *R.v.* laccase are shown in Figure 4A. A comparison of the corresponding FTs is shown in Figure 4B. The EXAFS data show a clear change in the beat pattern of the native intermediate relative to both the reduced and the oxidized samples. In particular, the native intermediate beat pattern is split in the region $k = 7-9$ $Å^{-1}$. More distinct differences can be seen in the comparison of the FTs. While the first shell amplitude of the native intermediate is slightly decreased relative to the oxidized sample, the outershell amplitude is dramatically increased relative to those of both the oxidized and the reduced samples. Figure S4 shows a comparison of the FTs of six separate preparations of the native intermediate relative to all of the preparations of oxidized and reduced laccase, indicating that the observed changes are clearly characteristic of the native intermediate form. These differences, as they relate to the fit results, will be considered below.

EXAFS fits to the data for the reduced, oxidized, and the native intermediate samples were performed using the 1.9 Å crystal structure of oxidized ascorbate oxidase as a starting model.[11] A good fit for reduced laccase was obtained by including three Cu−N/O interactions at 1.94 Å and multiple scattering interactions from the imidazole rings of the ligating histidines to fit the outer shells (Table 3, fit 1). As may be expected from the relatively low average coordination number, no improvement in the fit was obtained by inclusion of 0.25 Cu−S interactions corresponding to the short Cu−S (~2.1 Å) of the blue copper site; similar results were found for the oxidized and native intermediate data. The oxidized form was

(45) All other possible cases (Supporting Information Scheme S1) of the re-reduction of the native intermediate have been evaluated. In all cases, the calculated percentage of the Cu(I) present is overestimated as compared to the experimental values.

Table 2. Concentration and Percent Distribution of Species in the RFQ Samples[a]

sample		data (%)			model 1A			model 1B		model 2A			model 2B		
no.	[prot]/mM[b]	$Cu(I)_{tot}$[c]	$T1_{ox}$[d]	$T2_{ox}$[e]	fRed[f]	NI[g]	$Cu(I)_{cal}$[h]	fRed[f]	NI[g]	$fRED_{cal}$[i]	NI[g]	rNI_{cal}[i]	$fRed_{cal}$[j]	NI[g]	rNI_{cal}[j]
1[k]	0.4	17	78	0	22	78	42	22	78	−27	78	49	15	78	7
2[l]	0.4	23	38	0	62	38	72	62	38	−35	38	97	10	38	52
3[l]	0.4	25	53	0	47	53	60	47	53	−24	53	71	18	53	29
4	0.4	28	48	0	52	48	64	52	48	−20	48	72	20	48	32
5	0.4	8	68	0	32	68	49	32	68	−50	68	82	0	68	32
6	0.8	25	56	0	44	56	58	44	56	−22	56	66	19	56	25
7	0.6	8	75	0	25	75	44	25	75	−47	75	72	2	75	23

[a] RFQ samples were prepared in 100 mM phosphate buffer at pH 7.5, at 4 °C, unless otherwise stated. [b] Initial protein concentration with 96% RFQ packing efficiency. [c] % Cu(I) per total [Cu] according to the XAS edge data. Error (±10%). [d] % T1 Cu(II) per [protein] by EPR spin quantitation. Error (±7%). [e] % T2 Cu(II) per [protein] by EPR spin quantitation. Error (±7%). [f] % fully reduced (unreacted) by EPR spin quantitation 100% minus % T1 Cu oxidized. [g] % native intermediate by T1 Cu EPR spin quantitation. [h] % calculated Cu(I) per total [Cu] according to model 1A. [i] % calculated fully reduced (unreacted) and partially re-reduced native intermediate (rNI) according to model 2A. [j] % calculated fully reduced (unreacted) and partially re-reduced native intermediate (rNI) according to model 2B. [k] In MOPS pH 7.5. [l] Slight excess dithionite present as scrubbing agent in the mixing tubes.

Scheme 2

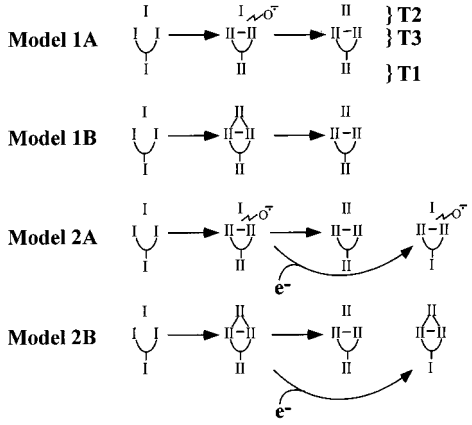

well fit by 3.5 Cu−N/O at 1.95 Å and outershell contributions from the imidazole rings (Table 3, fit 2). It should be noted that the increase in first shell coordination of the oxidized form is expected upon oxidation of the enzyme and is consistent with the increase in the first shell FT amplitude (Figure 4B). However, similar EXAFS fits are obtained with first shell coordination numbers between three and four.

In contrast to the oxidized and reduced samples, the native intermediate data are not well fit by inclusion of only Cu−N/O interactions and multiple scattering from histidine rings (Table 3, fit 3 and Figure S5A). As shown in Figure S5, there is clearly a large component of the outershell at ∼3.0 Å (nonphase shift corrected), which is not fit by typical histidine ring scattering. For this reason, an attempt was made to vary the orientation of the histidine rings. An improvement in the fit is obtained by splitting the Cu−N−Cα interactions into shorter and longer components at ∼3.0 and 3.3 Å. However, this fit (Table 3, fit 4) results in physically unreasonable σ^2 values. In addition, this distribution of distances requires a Cu−N distance of 2.1 Å with average Cu−N−Cα angles of 110° and 145° (vs ∼127° for a symmetrical bound histidine). Such a distortion of all of the histidine rings is unlikely. Attempts were also made to add Cu−C/N/O light atom interactions in addition to the histidine rings. However, to obtain a physically reasonable σ^2 value, an average of five Cu−C/N/O interactions at 3.40 Å were required (Table 3, fit 5). It is important to note that this is five interactions *per* copper, and is in addition to the histidine ring scattering. Such a model is not chemically reasonable. Having established that the outershell contribution to the EXAFS cannot be well fit by including only scattering from histidine or other light

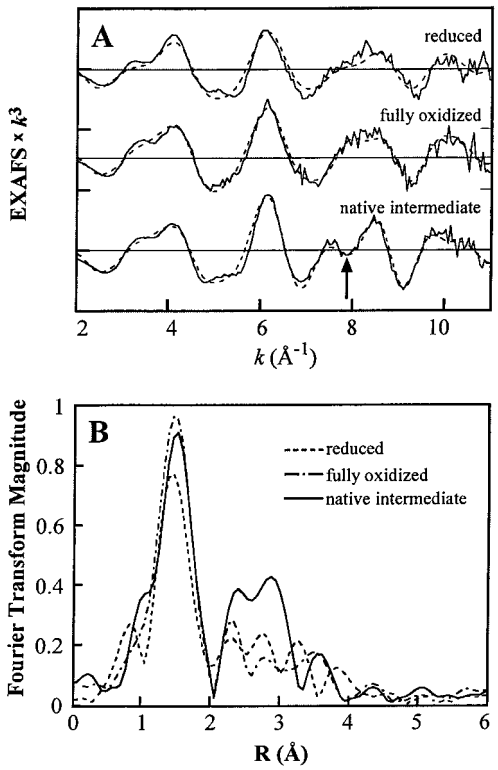

Figure 4. (A) Experimental EXAFS data (−) and fits to the data (- - -) for the reduced, fully oxidized, and native intermediate forms of laccase. Fit numbers 1, 2, and 6 (Table 3) are shown for data for the reduced fully oxidized, and native intermediate forms, respectively. (Each major tick on the ordinate scale represents five units.) (B) Nonphase shift-corrected Fourier transforms for reduced, fully oxidized, and native intermediate forms of laccase.

atoms, attempts were further made to fit the native intermediate outershell EXAFS data with inclusion of a Cu−Cu interaction. The results shown in Table 3, fit 6 and Figure S5B indicate that an excellent fit to the data is obtained. The data could be equally well fit by inclusion of either one Cu−Cu interaction (corresponding to two bridging interactions in the trinuclear cluster) or one and one-half Cu−Cu interactions (corresponding to three bridging interactions). However, it should be noted that inclusion of one-half Cu−Cu interactions resulted in a negative σ^2 value, indicating that the EXAFS data require at least two strong bridging interactions within the trinuclear cluster with a Cu−Cu distance of 3.3 Å.

5. MCD Spectroscopy. LT Spectra and Assignment. The LT MCD spectrum of the native intermediate in the energy

Table 3. EXAFS Fits to the Reduced, Fully Oxidized, and Native Intermediate Forms of Laccase

	reduced			fully oxidized			native intermediate											
fit no.	1			2			3			4			5			6		
ΔE_0	−8.35			−7.47			−7.28			−8.44			−7.78			−7.52		
	CN	R (Å)	σ^2 (Å^2)	CN	R (Å)	σ^2 (Å^2)	CN	R (Å)	σ^2 (Å^2)	CN	R (Å)	σ^2 (Å^2)	CN	R (Å)	σ^2 (Å^2)	CN	R (Å)	σ^2 (Å^2)
Cu−N/O	3	1.94	0.0085	3.5	1.95	0.0068	3.5	1.96	0.0083	3.5	1.94	0.0075	3.5	1.96	0.0075	3.5	1.96	0.0074
Cu−C[a]	5	2.95	0.0059	5	2.95	0.0068	5	2.99	0.0029	2.5	2.96	−0.0009	5	2.96	0.0027	5	2.96	0.0030
		3.04	0.0068		3.05	0.0073		3.08	0.0031		3.06	−0.0009		3.05	0.0029		3.05	0.0032
Cu−C[a]	5	3.95	0.0159	5	3.90	0.0059	5	3.96	0.0064	5	3.96	0.0041	5	3.96	0.0054	5	3.96	0.0078
		4.24	0.0186		4.19	0.0059		4.25	0.0064		4.25	0.0041		4.25	0.0054		4.25	0.0078
Cu−C[a]										2.5	3.32	0.0016						
											3.42	0.0016						
Cu−C/N													5	3.40	0.0015			
Cu−Cu																1	3.30	0.0032
Error[b]		0.250			0.194			0.405			0.310			0.183			0.153	

[a] These components represent a single scattering path (top) and the corresponding multiple scattering path (bottom). [b] Error is given by $\sum[(\chi_{obsd} - \chi_{calcd})^2 k^6]/\sum k^6 \chi_{obsd}^2$.

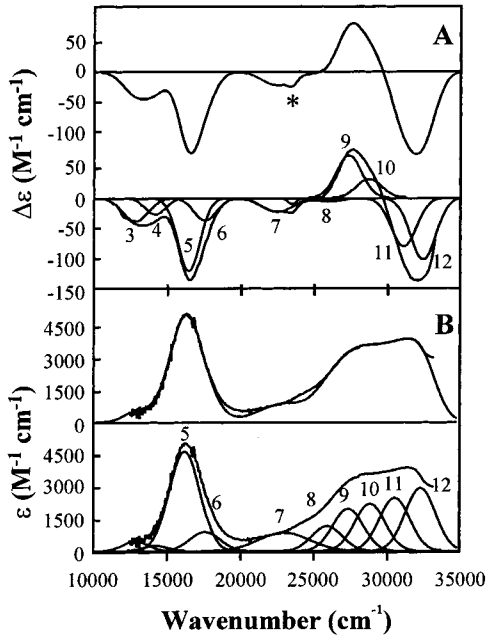

Figure 5. Simultaneous Gaussian fit of the native intermediate. (A) RT absorption spectrum and (B) LT MCD spectrum of the native intermediate is simultaneously fitted with a minimum number of Gaussian bands. * denotes a small amount of heme contaminant in the sample.

region of 10 000−35 000 cm^{-1} is shown in Figure S6. Panel A shows temperature dependence, and panel B shows the applied field dependence of the intermediate. The temperature and the field dependence are typical of MCD *C*-term behavior.[46] Consistent with our previously reported LT MCD spectrum of the native intermediate,[22] very intense apparent pseudo-A-shaped MCD features (two bands with equal intensity but opposite signs) are observed in the high-energy charge-transfer region with maxima at 316 nm (36 100 cm^{-1}) and 364 nm (27 500 cm^{-1}). In addition, LT MCD features associated with the oxidized T1 Cu center are visible in the low-energy region around 614 nm (16 300 cm^{-1}).

Simultaneous Gaussian fitting of the absorption and the MCD spectra for the native intermediate are included in Figure 5. As summarized in Table S2, a minimum of 12 bands is required to simultaneously fit both the RT Abs and the LT MCD spectra between 5000 and 33 300 cm^{-1}. The LT MCD spectrum of the native intermediate between 5000 and 10 000 cm^{-1} is shown in Figure S7. Assignments of bands 1 to 6 are based on analogy with other well-established absorption and MCD spectral assignments of the T1 copper site.[47,48] Bands 1 through 4 are assigned to ligand field transitions associated with T1 Cu center. Band 5 at 16 270 cm^{-1} is assigned to a Cys $S_{\pi} \rightarrow$ Cu $d_{x^2-y^2}$ CT transition. Band 6 at 17 780 cm^{-1} is assigned to a Cys $S_{\text{pseudo }\sigma} \rightarrow$ Cu CT transition. Band 7 at 22 050 cm^{-1} represents a number of unresolved bands involving charge-transfer transitions of histidine to the T1 copper and trinuclear copper centers. In the 25 000− 33 000 cm^{-1} region, the pseudo-A feature in the MCD spectrum (Figure 5A), in combination with the double peaked feature in the absorption spectrum (Figure 5B), requires at least two bands. However, from VTVH MCD spectral changes in the region (vide infra), there are actually five bands (8−12) required to fit the spectra and their changes in this region.

The relative band intensities in the MCD and the absorption spectra can differentiate between ligand field and charge-transfer transitions. For complexes exhibiting only *C*-term intensities, the C_0/D_0 ratio can be determined from the Gaussian fit of the MCD and the absorption spectra using the following equation.

$$\frac{C_0}{D_0} = \frac{k_B T}{\mu_B B}\left(\frac{\Delta\epsilon}{\epsilon}\right)_{max} \qquad (6)$$

where k_B is the Boltzmann's constant, μ_B is the Bohr magneton (k_B/μ_B = 1.489 K^{-1} T^{-1}), T is the temperature in Kelvin, ϵ is the molar absorptivity in M^{-1} cm^{-1}, and $\Delta\epsilon$ is the MCD intensity maximum measured in M^{-1} cm^{-1} taken within the linear 1/T region. The MCD intensities depend on the magnitude of the spin−orbit coupling parameter for the excited state. The spin−orbit coupling constant for the Cu (ξ_{3d}(Cu) = 828 cm^{-1}) is much greater than that for S (ξ_{3p}(S) = 382 cm^{-1}), N (ξ_{2p}(N) = 76 cm^{-1}), or O (ξ_{2p}(O) = 140 cm^{-1}).[49,50] Thus, d → d transitions tend to have much higher C_0/D_0 ratios than do charge-transfer transitions since they are centered on the Cu atom with a much larger spin−orbit coupling constant. For the T1 Cu center, bands 3 and 4, which are metal-based d → d transitions,

(46) Solomon, E. I.; Hanson, M. A. In *Inorganic Electronic Structure and Spectroscopy*; Solomon, E. I., Lever, A. P. B., Eds.; Wiley: New York, 1999; Vol. II, pp 1−129.
(47) Randall, D. W.; George, S. D.; Hedman, B.; Hodgson, K. O.; Fujisawa, K.; Solomon, E. I. *J. Am. Chem. Soc.* **2000**, *122*, 11620−11631.
(48) LaCroix, L. B.; Randall, D. W.; Nersissian, A. M.; Hoitink, C. W. G.; Canters, G. W.; Valentine, J. S.; Solomon, E. I. *J. Am. Chem. Soc.* **1998**, *120*, 9621−9631.
(49) Keijzers, C. P.; Boer, E. D. *Mol. Phys.* **1975**, *29*, 1007−1020.
(50) Blume, M.; Watson, R. E. *Proc. R. Soc. A* **1962**, *271*, 565−579.

show significantly higher C_0/D_0 ratios than do bands 5 and 6, which are Cys S → Cu charge-transfer transitions (Table S2). Bands 8 through 12 have |C/D| values of 0.02 to 0.09 (Table S2) which are within the range appropriate for CT.[51] Because the T1 does not contribute in this region, they are due to CT within the oxidized trinuclear cluster and would be associated with bridged μ-OH$^-$ (or μ-oxo, vide infra) to Cu(II) charge transfer.[38]

Saturation at Low Temperature. Normalized saturation magnetization curves taken at 31 780 and 27 560 cm^{-1} are shown in Figure S8. These were obtained by increasing the magnetic field at fixed temperature at 1.8 K. These curves are dependent on the S_{tot} of the ground state in the limit of no zero field splitting (ZFS). The normalized magnetization curves, M, for different possible spin states are included in the figure (solid lines). These were generated using the Brillouin function, $B_S(x)$, for a ground state with spin = S (eq 7).

$$M = NgS\beta B_S(x) \tag{7A}$$

$$B_S(x) = \left[\frac{2S+1}{2S}\coth\left(\frac{2S+1}{2S}x\right) - \frac{1}{2S}\coth\left(\frac{1}{2S}x\right)\right] \tag{7B}$$

In eq 7A, x is $gS\beta H/k_BT$, N is Avogadro's number, S is a given spin state, β is the Bohr magneton (9.274 × 10^{-24} J T^{-1}), H is the applied field in Tesla, k is Boltzmann's constant (1.381 × 10^{-23} J K^{-1}), and T is temperature in Kelvin. These simulations clearly show that the ground state is $S = {}^1/_2$ with g = 2.19 (31 780 cm^{-1} band) and 2.14 (27 560 cm^{-1} band). This assignment of the ground state to $S = {}^1/_2$ from the saturation magnetization data is in agreement with the observation of frequency independent g values from EPR spectroscopy in Figure S1.

VTMCD: Excited-State Analysis. Figure 6A shows the MCD spectrum (expanded scale) of the native intermediate in the high-energy region (22 200−35 000 cm^{-1}) between 5 and 170 K. MCD transition intensity of a magnetically isolated system normally decreases as temperature increases, that is, intensity ∝ 1/T. This behavior is observed in the T1 features and in the heme contaminant at 23 500 cm^{-1}. However, the bands in Figure 6A show spectral changes indicating thermal population of an excited state with a different MCD spectrum. This is demonstrated by the temperature dependence of the MCD signal taken at different energies. The plot in Figure 6B taken at 25 000 cm^{-1} (arrow in panel A) clearly exhibits the contributions from both the ground and the first excited state. At temperatures between 0 and 30 K, the band intensity rapidly decreases. However, between 40 and 100 K, the intensity starts to increase indicating increasing contribution from an excited state with a larger positive MCD signal than the ground state. At temperatures above 150 K, the band intensity starts to decrease again indicating thermal population of a second excited state. This decrease is faster than 1/T, which would be expected without the presence of a higher excited state. Attempts to increase the temperature above 170 K cause a phase transition of the glass, which prevented further analysis.

The total intensity of the MCD spectrum of a system with thermally accessible excited states is given by the Boltzmann

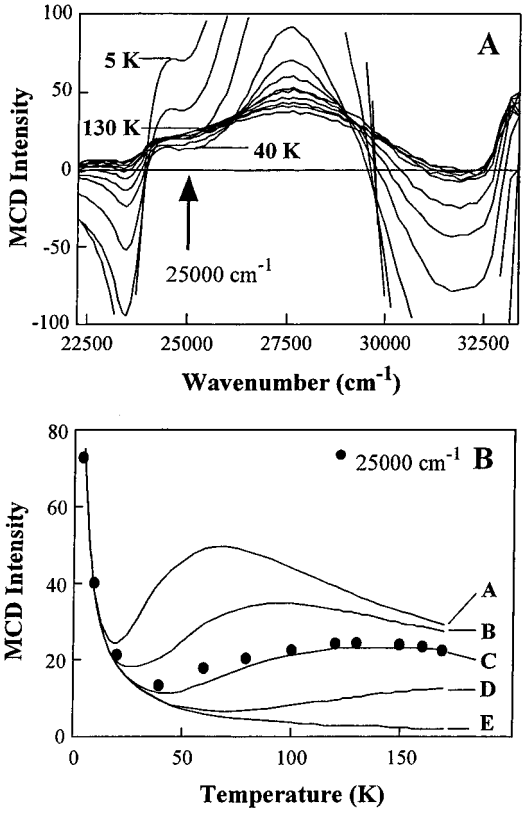

Figure 6. (Panel A) The temperature dependence of the native intermediate MCD spectra. The intensity of the signal decreases between 5 and 40 K but rises again at higher temperatures, 50−150 K. (Panel B) The temperature dependence of the native intermediate MCD spectra at 25 000 cm^{-1} (●) in panel A. Solid lines are generated according to eq 7 assuming the following energy parameters. A, 70 cm^{-1}, 175 cm^{-1}; B, 100 cm^{-1}, 250 cm^{-1}; C, 150 cm^{-1}, 350 cm^{-1}; D, 250 cm^{-1}, 625 cm^{-1}; and E, isolated (1000 cm^{-1}, 1000 cm^{-1}) for the relative energies of the first and the second excited states (see text).

population of these states each having a C term that decreases as 1/T. Thus, the energy separation (ΔE) between the states is obtained by fitting the temperature dependence of the MCD intensity at any given wavelength (λ) according to eq 8.

$$I_{MCD}(\lambda) = \frac{\sum_i \left(\mathrm{Deg}_i \exp\left(\frac{-E_i hc}{k_BT}\right) C_i \frac{1}{T}\right)}{\sum_j \left(\mathrm{Deg}_j \exp\left(\frac{-E_j hc}{k_BT}\right)\right)} \tag{8}$$

where i and j are the different spin states, $\mathrm{Deg}_{i \text{ or } j}$ is the degeneracy of the state (i or j), $E_{i \text{ or } j}$ is its energy, h is Planck's constant (6.626 × 10^{-34} J s), c is the speed of light (2.998 × 10^{10} cm s^{-1}), k_B is Boltzmann's constant (1.38 × 10^{-23} J K^{-1}), and T is the temperature in Kelvin. The degeneracy of each state is 2 for the ground state ($S = {}^1/_2$) and the first excited state ($S = {}^1/_2$) and 4 for the second excited state ($S = {}^3/_2$) (vide infra). C_i is the MCD intensity of state i at wavelength λ.

For the simulation of the temperature dependence of the MCD spectrum for the native intermediate, the C-term coefficients for the ground state ($C_{i = \text{ground state}}$) were fixed by using the 1.8 K MCD spectrum of the native intermediate scaled by the temperature. There are no changes in the MCD spectra between 1.8 and 2.5 K, which indicates that only the ground state is

(51) Gewirth, A. A.; Solomon, E. I. *J. Am. Chem. Soc.* **1988**, *110*, 3811−3819.

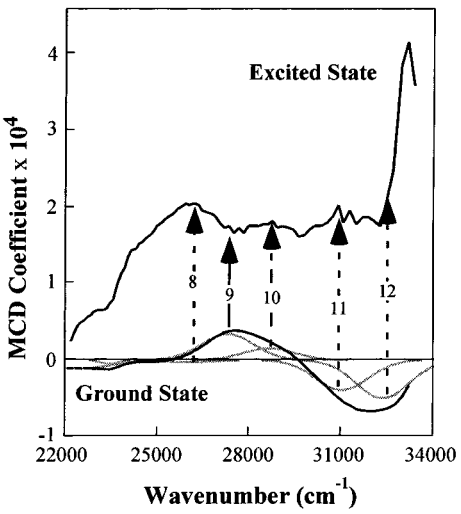

Figure 7. The ground- and excited-state MCD spectra of the native intermediate. Gaussian fit of the ground-state spectrum is shown in gray. Different arrows indicate the different Cu_i associated with the CT transitions (see Figure 10).

thermally populated at 1.8 K. The excited-state spectral contribution of the native intermediate was obtained by floating the energy parameter E_i and the first excited state *C*-term coefficient ($C_{i\,=\,\text{first excited state}}$). The best fit was achieved as shown by line C in Figure 6B with 150 cm^{-1} for the first excited state and 350−900 cm^{-1} for the second excited state. Addition of the *C*-term coefficient for the second excited state ($C_{i\,=\,\text{second excited state}}$) to the fitting routine did not improve the goodness of the fit; however, it was necessary to include the energy separation for its effect on the population of the first excited state. The energy separation between the ground and the first excited state of 150 cm^{-1} is in excellent agreement with the Δ value obtained from the Orbach analysis of the temperature dependence of the EPR (see section Power Saturation and Orbach Analysis). Furthermore, the MCD spectrum of the first excited state could be generated from the wavelength dependence in the *C*-term coefficients (C_i in eq 8) obtained by simulating the temperature dependence at each wavelength fixing the energy separation between the ground and the first excited state at 150 cm^{-1}. Figure 7 shows the resultant MCD spectra of the first excited state and the ground states of the native intermediate.

From Figure 7, there are five bands in the high-energy region between 25 000 and 33 000 cm^{-1}, which indicate the presence of multiple charge-transfer transitions associated with the trinuclear Cu(II) cluster. Band 8 is fit with a small negative peak in the ground state that changes sign and gains intensity in the excited state.[52] Band 9 is very intense and positive in the ground state. This band decreases in intensity in the excited state. Band 10 is apparent in the ground state as a shoulder but gains MCD intensity in the excited state. Band 11 is an intense negative band in the ground state. This band changes sign and gains intensity in the first excited state. Band 12 is difficult to assign due to the close energy proximity to the protein absorption. However, this band reproducibly changes sign and gains intensity in the excited state.

6. Exchange-Coupling Models. The spectroscopic data presented here limit the structural possibilities of the native intermediate. These restrictions are as follows: (1) All Cu atoms

Chart 1. (A) Coupling Scheme for the Trinuclear Cu(II) Cluster and (B) A Model for the Native Intermediate with Three Coupling Constants

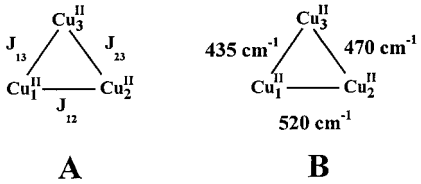

are oxidized in the native intermediate. (2) The frequency dependence of the *g*-values from multifrequency EPR spectroscopy and the Brillouin function fit to the saturation magnetization MCD intensity at low temperature indicate that the ground state is $S_{tot} = {}^1/_2$. (3) VT MCD and the Orbach analysis of the EPR relaxation show that the first excited state is thermally accessible at 150 cm^{-1}. (4) EXAFS analysis indicates a Cu−Cu interaction present in the native intermediate at 3.3 Å, which is not present in resting oxidized laccase. This distance requires that there cannot be two single atom bridges between two Cu atoms. (5) The temperature dependence of the MCD data shows that the MCD spectrum of the 150 cm^{-1} excited state is different from that of the ground state (Figure 7).

A number of possible structural models for the trinuclear Cu cluster of the native intermediate are considered below. A model is considered acceptable when it is consistent with all the above spectroscopic data. First, a single-bridge model in which two Cu(II) atoms form a coupled binuclear center with the third Cu(II) atom in an isolated state is considered (equivalent to the resting oxidized state in Scheme 1). Second, a two-bridge model is considered where the third Cu(II) center is coupled to one of the binuclear copper ions. Finally, a three-bridge model is considered in which the spins on all three copper atoms are exchange-coupled.

For an exchange-coupled trinuclear Cu(II) complex, the general spin Hamiltonian is

$$H = -2J_{12}S_1\cdot S_2 - 2J_{23}S_2\cdot S_3 - 2J_{13}S_1\cdot S_3 \qquad (9)$$

where J_{12}, J_{23}, and J_{13} are exchange-coupling constants between the neighboring copper ions indicated.[53−56] Each spin can interact with its adjacent neighboring spins in the trimer as shown in Chart 1A. Two Cu(II) atoms with $S = {}^1/_2$ couple to form intermediate spins $S_{tot} = 1$ and 0. The $S_{tot} = 0$ couples to the third copper atom with $S = {}^1/_2$ to give the $|{}^1/_2, 0\rangle$ state. The $S = 1$ couples to the third Cu(II) atom to give $S_{tot} = |{}^3/_2, 1\rangle$ and $|{}^1/_2, 1\rangle$ states. The energies of these spin levels of the trimer are given by the matrix shown in Table S3.[54]

Single-Bridge (1J) Model. Figure 8A shows the energy levels of the three spin states for the single- or two-bridge model as a function of the J_{23}/J_{12} ratio. The single-bridge trimer model consists of two antiferromagnetically coupled spins with the third

(52) Gaussian fitting routinely results in a small negative peak for band 8. However, since band 8 in the ground state is obscured by the neighboring bands, a small positive band will also fit the data with an acceptable σ^2 value. This does not affect the analysis.
(53) Cole, J. L.; Clark, P. A.; Solomon, E. I. *J. Am. Chem. Soc.* **1990**, *112*, 9534−9548.
(54) Bencini, A.; Gatteschi, D. *Electron Paramagnetic Resonance of Exchange Coupled Systems*; Springer-Verlag: Berlin, New York, 1990.
(55) Banci, L.; Bencini, A.; Gatteschi, D. *Inorg. Chem.* **1983**, *22*, 2681−2683.
(56) Banci, L.; Bencini, A.; Dei, A.; Gatteschi, D. *Inorg. Chem.* **1983**, *22*, 4018−4021.

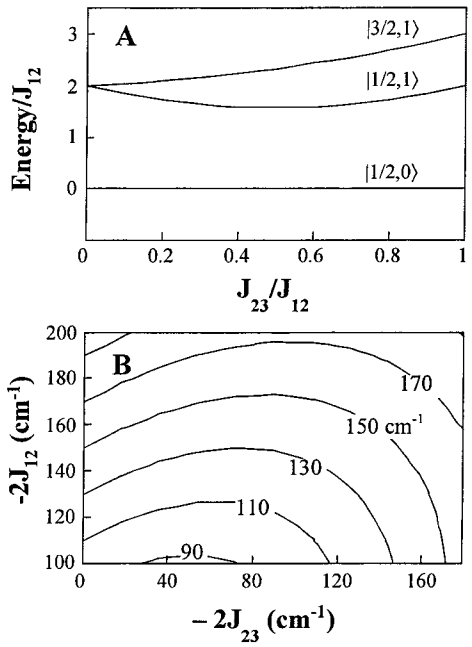

Figure 8. The energy diagram and the solution space for the two-bridge model. (Panel A) Energy levels of the trimer in terms of J_{23}/J_{12}, while J_{13} is fixed to zero. (Panel B) Solution space for $-2J_{12}$ and $-2J_{23}$ that allows energy separation of the ground and the first excited state as labeled.

spin magnetically isolated (i.e., $J_{23}/J_{12} = 0$). This model describes the resting oxidized state of the trinuclear Cu cluster. Here, the two spin states from $S'=1$ are degenerate and are separated from the ground-state $S' = 0$ by $-2J$. This model predicts that the isolated Cu(II) center in the native intermediate will exhibit a number of spectroscopic characteristics that are similar to the T2 Cu(II) center in resting oxidized laccase. However, the spectroscopic data of the native intermediate do not support this model.

Two-Bridge (2J) Model. A two-bridge model, which is analogous to a linear trimer, is considered next. In this case, the coupling between the center atom and the two terminal Cu(II)s is nonzero, while the coupling between the outer Cu(II) ions is set to zero. This results in three spin levels at different energies with the $|^1/_2, 0\rangle$ state (i.e., $S_{tot} = 1/2$) as a ground state. The energy separation of the two excited states, $|^1/_2, 1\rangle$ and $|^3/_2, 1\rangle$, above the ground state in the two-bridge model is given as a function of the coupling constant ratio in Figure 8A. In the limiting symmetrical case where the two coupling pathways are comparable (i.e., $J_{23}/J_{12} \approx 1$), $|^1/_2, 1\rangle$ and $|^3/_2, 1\rangle$ states are above the ground state by $2J$ and $3J$, respectively. The first excited-state energy calculated as a function of the two coupling constants is given in Figure 8B. The solution space for the first excited state at 150 cm^{-1} shows the maximum allowed $-2J$ value for J_{12} and J_{23} is $\leq$170 cm^{-1}.

While this model fulfills the requirement of a doublet ground state and a 150 cm^{-1} energy separation for the first excited state, *the coupling constants of <170 cm^{-1} are inconsistent with the Cu−Cu distance determined by EXAFS*. From systematic studies on model complexes, Hatfield and co-workers have found that the exchange-coupling constant of Cu−OH−Cu complexes strongly depends on Cu−O−Cu angle which in turn relates to Cu−Cu distance.[57−59] Figure 9 shows the magnetostructural

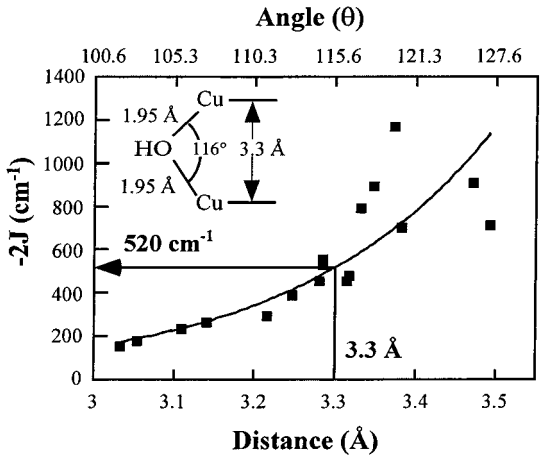

Figure 9. Magnetostructural correlation of the Cu−Cu distance and angle with coupling constants for OH bridged binuclear Cu(II) model complexes. A Cu−O distance of 1.95 Å is assumed as shown in the inset. Note that there is a nonlinear relationship between the Cu−O−Cu angle (θ) and the Cu−Cu distance (Å). Data taken from Tandon et al. *Inorg. Chem.* **1994**, *33*, 5555−5570.

correlation between the $-2J$ values and Cu−Cu distance. (Note: This has been converted from Cu−OH−Cu angle based on the scheme shown in the inset.) The EXAFS distance of the native intermediate, 3.3 Å, requires a large $-2J$ value of ~520 cm^{-1}. The fact that the EXAFS shows a clear outer shell Cu−Cu interaction requires a favorable Debye−Waller factor and a strong bridge. Thus, the EXAFS-determined Cu−Cu distance requires a magnitude of $-2J$ that exceeds the allowed maximum coupling constant for the single- or two-bridge models for the native intermediate.

Three-Bridge (3J) Model. A three-bridge model in which each spin in a triad is coupled to two neighboring spins is now considered. Figure S9 shows the solution space for the energy of the first doublet at 150 cm^{-1} for different values of $-2J$ for all three bridges. With J_{12} defined as the largest, the bold line in Figure S9 represents a coupling scheme that satisfies all experimental constraints. The $-2J = 520$ cm^{-1} curve allows one of the $-2J$ values to vary from 445 to 520 cm^{-1}, while the other $-2J$ stays near 440 cm^{-1}. (This model assumes the EXAFS-determined Cu−Cu distance at 3.3 Å reflects the strongest bridge; thus, the largest coupling is limited to 520 cm^{-1}.) The EXAFS restriction (Cu−Cu = 3.3 Å and $-2J =$ 520 cm^{-1}) can be fulfilled along with the doublet excited state at 150 cm^{-1} if both $-2J_{13}$ and $-2J_{23}$ are large and comparable to $-2J_{12}$.

7. Coupling Coefficients from VT MCD. The range of the coupling constants in case III can be further refined by considering the spectral changes between the ground state and the first excited doublet state of the native intermediate. The MCD *C*-terms represent contributions from electronic transitions centered on the three individual Cu(II) ions, and the total MCD intensities are weighted by the coupling coefficients of the individual coppers into the trinuclear wave functions, $c_{(i)}$.[53] The MCD *C*-terms associated with the ground doublet state (i.e., $|^1/_2, 0\rangle$) and the first excited doublet state (i.e., $|^1/_2, 1\rangle$) are then given by the following equations.

(57) Thompson, L. K.; Lee, F. L.; Gabe, E. J. *Inorg. Chem.* **1988**, *27*, 39−46.
(58) Crawford, V. H.; Richardson, H. W.; Wasson, J. R.; Hodgson, D. J.; Hatfield, W. E. *Inorg. Chem.* **1976**, *15*, 2107−2110.
(59) Tandon, S. S.; Thompson, L. K.; Manuel, M. E.; Bridson, J. N. *Inorg. Chem.* **1994**, *33*, 5555−5570.

$$C_o\left(\frac{1}{2},0\right) = c_1C_{0(1)} + c_2C_{0(2)} + c_3C_{0(3)} \qquad (10A)$$

$$C'_o\left(\frac{1}{2},1\right) = c'_1C'_{0(1)} + c'_2C'_{0(2)} + c'_3C'_{0(3)} \qquad (10B)$$

where the $C_{0(i)}$ and $C'_{0(i)}$ refer to the *C*-terms associated with electronic transitions at each of the three copper centers in the trinuclear cluster in the $|^1/_2, 0\rangle$ and the $|^1/_2, 1\rangle$ state, respectively.

The $|^1/_2, 0\rangle$ ground-state coefficients are given by eq S1, while the $|^1/_2, 1\rangle$ excited-state coefficients are given by eq S2. Experimentally, the MCD temperature dependence of the native intermediate between 25 000 and 33 000 cm^{-1} shows at least five bands with three different behaviors (Figure 7). Band 10 (28 700 cm^{-1}) is positive in both the ground and the excited states. Band 9 at 27 300 cm^{-1} is large and positive in the ground state but loses much of its intensity in the excited state. Bands 8 (26 000 cm^{-1}), 11 (31 000 cm^{-1}), and 12 (32 400 cm^{-1}) are negative in the ground state but large and positive in the excited state. These differences can be explained in terms of differences in the wave functions of the two states as shown in Figure 10 obtained from eqs S1 and S2. The MCD spectral intensities of the native intermediate arise from the summation of the $c_{(i)}$ coefficient weighted electronic transitions from each of the three coppers. Accordingly, bands 8, 11, and 12 are charge-transfer transitions to Cu_2(II), band 10 to Cu_1(II), and band 9 to Cu_3(II). Moreover, correlation of the experimental spectral differences with the wave function changes between the ground and the excited state allows an estimate of the three coupling constants in the native intermediate (Chart 1B). Note that these assume one *J* value of 520 cm^{-1} from the EXAFS analysis.

8. EPR Trimer *g* Values. The observed *g* values (2.15, 1.85, and 1.65) of the native intermediate are different from those of the resting trinuclear cluster and are unusual for a Cu(II) complex in that two of the *g* values are significantly below the spin-only value of 2.0023. However, the observed *g* values arise from an all-coupled trimer Cu(II) cluster. The resting oxidized form has two Cu(II) atoms coupled in the T3 center so that spin is localized on T2 Cu(II). As described by eq 11, the observed *g*-tensor is constructed from a linear combination of the local monomeric *g*-tensors weighted by the same c_i coupling coefficients as in eq 10 and determined from the MCD studies.

$$g\left(\frac{1}{2},0\right) = c_ag_{(a)} + c_bg_{(b)} + c_cg_{(c)} \qquad (11)$$

A number of different cases can be considered for local *g*-tensors in which the three local copper atoms all have $d_{x^2-y^2}$ ground states, d_{z^2} ground states, or a combination. For each possibility, a number of permutations of the *g*-tensor orientations and three coupling coefficients must be considered to reproduce the observed trimer *g* values. This approach gives a set of two *g* values slightly below 2.0023, but the third is much larger than the observed g_{max} (Figure S10A).

Alternatively, two of the local Cu(II) centers can be fixed with a set of *g* values, while the local *g*-tensor of the third center is allowed to vary to fit the experimental *g* values. It is found that when two local copper centers are assumed to have a $d_{x^2-y^2}$ and a d_{z^2} ground state (or two $d_{x^2-y^2}$ ground states), the observed trimer *g* values can be reproduced if the third Cu(II) atom (Cu_1 with the large positive coupling coefficient) has local *g* values of 1.41, 1.55, and 0.56 (Figure S10B). These are similar to those observed experimentally for a copper doped in ZnO in which the site symmetry is close to tetrahedral.[60] This leads to a small splitting of the $^2T_2$ ground state of the Cu(II) center and a significant orbital angular momentum contribution to the *g* values. Thus, it appears that there are structural constraints on one copper atom in the trinuclear cluster of the native intermediate, which limit the Jahn−Teller distortion of the Cu(II). This likely relates to the all-bridged structure of the trinuclear cluster in the native intermediate.

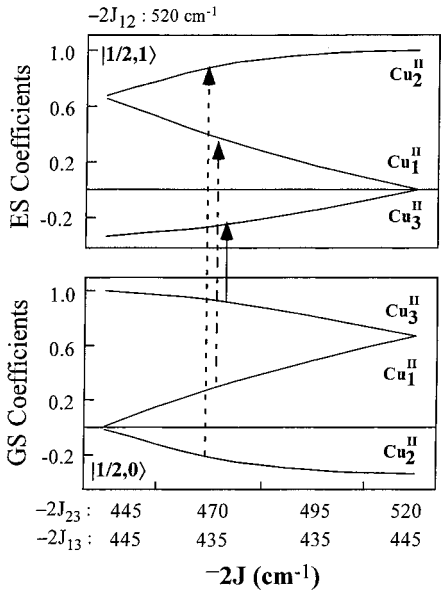

Figure 10. Coupling coefficients of the individual coppers of the trinuclear Cu(II) cluster in the ground state (GS) and excited state (ES) wave functions. Different arrows indicate the different copper associated with the CT transitions according to the coupling scheme (see text).

IV. Discussion

1. Structural Model. This study has shown that four-electron reduced laccase reacts with O_2 to give the native intermediate in which all the copper atoms are oxidized, similar to the redox states of the resting oxidized form. This is clearly shown by the Cu K-edge XAS of the native intermediate. Moreover, the absorption and MCD data of the native intermediate also show it cannot involve a hydroxyl radical. Spectroscopic data of this radical species trapped in an argon matrix exhibit very different features[61] from that of the native intermediate (Figure S11). The lack of the T2 Cu EPR signal in the native intermediate misled past researchers to believe that this site is reduced, and many assumed a hydroxyl or oxyl radical species for the native intermediate. However, it is clear from this study that T2 copper in the native intermediate is not EPR silent but is involved in coupling to the T3 coppers that greatly changes the signal.

Although the redox states of the native intermediate and resting oxidized laccase are equivalent, the two forms have very different geometric structures. The new bridging interaction present in the EXAFS spectrum with a Cu−Cu interaction at 3.3 Å differentiates the native intermediate from the resting oxidized form. Another dramatic difference is obtained from

(60) Dietz, R. E.; Kamimura, M. D.; Sturge, M. D.; Yariv, A. *Phys. Rev.* **1963**, *132*, 1559−1569.
(61) Langford, V. S.; Williamson, B. E. *J. Phys. Chem. A* **1997**, *101*, 3119−3124.

Chart 2. Structural Models of the Native Intermediate. ((A) All Three Copper Atoms Bridged by Hydroxide and (B) All Bridged by a Single μ_3-Oxo)

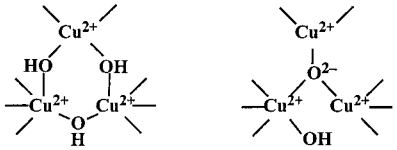

A **B**

the temperature dependence of the MCD spectrum and the Orbach analysis of the EPR saturation data that show a low-lying excited state at 150 cm^{-1} for the native intermediate. This combined with the EXAFS-determined Cu−Cu distance, which is consistent only with a large coupling constant around 520 cm^{-1}, require a three-bridge model for the native intermediate. Here, spin-exchange coupling of all three coppers results in a spin-frustrated system giving a low-lying excited state at 150 cm^{-1} with large individual exchange couplings.

Two possible structural models are shown in Chart 2 in which the O−O bond has been broken in the formation of the native intermediate. Chart 2A shows a structure with all three copper atoms bridged by hydroxide. In this model, both oxygen atoms from O_2 are still bound to the trinuclear copper cluster. Alternatively, Chart 2B shows a structure with three Cu centers all bridged by a single μ_3-oxo. In this model, the second oxygen atom of the dioxygen is already dissociated from the trinuclear cluster as H_2O.

2. Mechanistic Implications. The decay of the native intermediate to the resting oxidized state is very slow (Scheme 1, 0.034 s^{-1}).[21] In fact, this process is slower than the overall turnover number such that this step cannot be catalytically competent. The reported turnover number ranges[62] from 0.13 to 560 s^{-1}. Accordingly, it was proposed that a direct reduction of the native intermediate to the fully reduced state occurs during the catalytic cycle. Structural definition of the native intermediate provides insight into the origin of this slow decay. ^{17}O-EPR[27,63] and ^{18}O-IRMS[18,64] results indicate that only one oxygen atom from O_2 is present in resting oxidized laccase (decayed product), and it is a water or OH^- bound to T2 Cu(II). The crystal structure of the resting oxidized state shows that this water (or OH^-) is terminally bound and oriented away from the interior of the trimer.[11,15] In the native intermediate, however, the oxygen atom(s) of dioxygen is(are) bridging the trimer. Thus, the decay of the native intermediate to the resting oxidized state would require a large structural reorganization of one of the oxygen atoms from the interior to the exterior of the trimer.

Another complicating factor is that the intramolecular ET from the T1 center to the trinuclear cluster in the resting oxidized enzyme is very slow. This process has been measured directly using pulse radiolysis or laser flash photolysis in laccase[65] or in ascorbate oxidases.[66−69] In laccase, the measured rate constant of ~1 s^{-1} (independent of the extent of T1 Cu reduction and of the substrate concentration) is much slower than the observed maximal overall turnover number of 560 s^{-1}. Thus, the intramolecular electron transfer rate between the T1 center and the trinuclear cluster is partially inactivated and must be faster under turnover conditions. It was shown that the slow intramolecular ET could be partially activated after a single turnover[70] or in the presence of the dioxygen during multiple turnovers.[71] Further, this activation slowly returns to an inactivated form with a decay rate constant that matches that of the native intermediate decay to the resting oxidized state.[70] Thus, it is proposed that under turnover conditions, the native intermediate is the primary acceptor of reducing substrates rather than the resting oxidized form.

The increase in the reduction rate of the trinuclear cluster in the native intermediate would be consistent with having strongly coupling bridges between the copper ions in the trinuclear cluster. On the other hand, the slow reduction rate of the trinuclear cluster in the resting oxidized form is consistent with having the magnetically isolated nonbridged T2 copper. In ceruloplasmin, no efficient ET pathway from the surface or T1 center to the T2 Cu is present in the resting oxidized state,[72] and thus the T2 center is very difficult to reduce. However, in the native intermediate, since all Cu atoms are bridged, the electronic coupling (H_{DA}) would be much more favorable for rapid ET through the cluster.[73,74] Moreover, since the $E°$ of the trinuclear cluster in the native intermediate is expected to be higher than that of the resting oxidized site (the native intermediate is unstable and decays to the resting oxidized form), a larger driving force is expected for the ET process. Note that while the additional bridging in the native intermediate relative to the resting state increases ET through mainly H_{DA} and $E°$, the reorganization energy (λ) would increase as more bonds are broken on reduction. This would have an adverse effect on the ET rate and is thus a small contributor relative to H_{DA} and $E°$. Thus, under turnover conditions, it appears that direct reduction of the native intermediate occurs in the catalytic mechanism. One feasible model for reduction of the native intermediate is shown in Scheme 3. The reducing substrate delivers the first equivalent to the active site via the T1 center in the anaerobic reduction of the resting oxidized enzyme or re-reduction of the native intermediate. In ceruloplasmin, reduction of the resting oxidized form was clearly shown to involve a second substrate together with the reduced T1 copper center resulting in a two-electron reduction of the T3 copper atoms.[72] It was further shown that the T2 Cu is the last to be reduced. In the re-reduction process of the native intermediate,

(62) The specific activities of Lc under a similar condition differ substantially among different preparations by different research groups. It has been reported by Petersen and Degn (Petersen, L. C.; Degn, H. *Biochim. Biophys. Acta* **1978**, *526*, 85−92) that slow substrates do not saturate and show substrate-dependent turnover numbers of 1170 M^{-1} s^{-1} for hyrodroquinone and 259 M^{-1} s^{-1} for ascorbate. Others have reported substrate saturation with ascorbate, but the reported turnover numbers vary a great deal: 0.13 s^{-1} by Hansen et al. (Hansen, F. B.; Noble, R. W.; Ettinger, M. J. *Biochemistry* **1984**, *23*, 2049−2056), 8.5 s^{-1} by O'Neill et al. (O'Neill, P.; Fielden, E. M.; Morpurgo, L.; Agostinelli, E. *Biochem. J.* **1984**, *222*, 71−76), and 117 s^{-1} by Tollin et al. (Tollin, G.; Meyer, T. E.; Cusanovich, M. A.; Curir, P.; Marchesini, A. *Biochim. Biophys. Acta* **1993**, *1183*, 309−314) under the similar reaction condition. The maximal turnover number for *Rhus* laccase is reported to be 560 s^{-1} with phenylenediamine at pH 7.4 and 25 °C.

(63) Brändén, R.; Deinum, J. *FEBS Lett.* **1977**, *73*, 144−146.
(64) Brändén, R.; Deinum, J.; Coleman, M. *FEBS Lett.* **1978**, *89*, 180−182.
(65) Farver, O.; Pecht, I. *Mol. Cryst. Liq. Cryst.* **1991**, *194*, 215−224.
(66) Meyer, T. E.; Marchesini, A.; Cusanovich, M. A.; Tollin, G. *Biochemistry* **1991**, *30*, 4619−4623.
(67) Farver, O.; Pecht, I. *Proc. Natl. Acad. Sci. U.S.A.* **1992**, *89*, 8283−8287.
(68) Kyritsis, P.; Messerschmidt, A.; Huber, R.; Salmon, G. A.; Sykes, A. G. *J. Chem. Soc., Dalton Trans.* **1993**, *5*, 731−735.
(69) Hazzard, J. T.; Marchesini, A.; Curir, P.; Tollin, G. *Biochim. Biophys. Acta* **1994**, *1208*, 166−170.
(70) Hansen, F. B.; Koudelka, G. B.; Noble, R. W.; Ettinger, M. J. *Biochemistry* **1984**, *23*, 2057−2064.
(71) Farver, O.; Wherland, S.; Pecht, I. *J. Biol. Chem.* **1994**, *269*, 22933−22936.
(72) Machonkin, T. E.; Solomon, E. I. *J. Am. Chem. Soc.* **2000**, *122*, 12547−12560.
(73) Marcus, R. A.; Sutin, N. *Biochim. Biophys. Acta* **1985**, *811*, 265−322.
(74) Marcus, R. A. *Biochim. Biophys. Acta* **1985**, *811*, 405−405.

Scheme 3

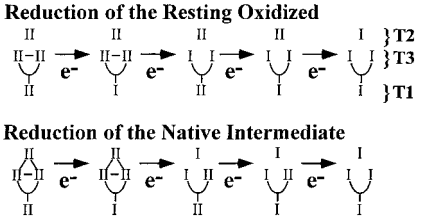

a similar two-electron process would now be able to reduce the T2 and one of the T3 copper atoms, since the three Cu atoms are linked by a strong exchange-coupling pathway that provides rapid ET. This model predicts formation of a mixed valence T3 copper center. Indeed, it was found that the native intermediate decays in the presence of excess reductant to a species with a new Cu signal that was assigned as a half-reduced T3 signal.[75,76] Further reduction of the remaining T3 center in the native intermediate should be fast via the Cys/His pathway between the T1 and T3 centers. In contrast, this reduction in the resting oxidized is very slow since the T2 Cu center is buried and electronically isolated.

V. Conclusions

This study has shown that the native intermediate has all coppers oxidized. Furthermore, all three copper atoms in the trinuclear cluster are strongly coupled by bridged hydroxide or oxo groups. This causes spin frustration, which allows thermal population of a low-lying excited spin state, which can be probed by EPR relaxation and temperature dependence MCD spectroscopy. On the basis of the observed spectroscopic properties, a clearly defined structural model for the native intermediate has been developed. In-depth knowledge of this intermediate provides structural insight into the unusual kinetic behavior observed for the multicopper oxidases. The slow decay of the native intermediate to the resting oxidized laccase can be understood in terms of a large structural change associated with loss of the bridging product of O_2 reduction. In addition, the rapid rate of re-reduction of the native intermediate as compared to that of the resting oxidized enzyme can be explained by the strong electronic coupling among the copper atoms in the trinuclear cluster. This couples all three copper atoms into a superexchange pathway allowing fast ET between the T1 center and the trinuclear cluster in catalytic turnover.

Acknowledgment. We thank Mr. Andrew Skulan for helpful discussions regarding exchange-coupling models, Dr. Frank Neese for his EPR simulation program, and Prof. John D. Lipscomb for allowing use of a stopped-flow instrument. This research was supported by NIH Grants DK31450 (E.I.S.) and NIH RR-01209 (K.O.H.). SSRL operations are funded by the Department of Energy, Office of Basic Energy Sciences. The SSRL Structural Molecular Biology program is supported by the National Institutes of Health, National Center for Research Resources, Biomedical Technology Program, and by the Department of Energy, Office of Biological and Environmental Research.

Supporting Information Available: Experimental spectroscopic parameter summary table; the spin level energy matrix and coefficient equations; alternative re-reduction scheme; and figures showing spectroscopic characteristics of the native intermediate including multifrequency EPR spectra, simulations, and power saturation data, detailed EXAFS and VTVH MCD spectra, calculated coupling constant solution space for the three-bridge model, and calculated trimer g-values. (PDF). This material is available free of charge via the Internet at http://pubs.acs.org.

JA0114052

(75) Reinhammar, B. *J. Inorg. Biochem.* **1981**, *15*, 27−39.
(76) Reinhammar, B.; Malkin, R.; Jensen, P.; Karlsson, B.; Andréasson, L.-E.; Aasa, R.; Vänngård, T.; Malmström, B. G. *J. Biol. Chem.* **1980**, *255*, 5000−5003.